Octant analysis based structural relations for three-dimensional turbulent boundary layers

Semih M. Ölçmen, Roger L. Simpson, and Jonathan W. Newby

Citation: Physics of Fluids (1994-present) **18**, 025106 (2006); doi: 10.1063/1.2172650
View online: http://dx.doi.org/10.1063/1.2172650
View Table of Contents: http://scitation.aip.org/content/aip/journal/pof2/18/2?ver=pdfcov
Published by the AIP Publishing

Octant analysis based structural relations for three-dimensional turbulent boundary layers

Semih M. Ölçmen
Department of Aerospace Engineering and Mechanics, The University of Alabama, Tuscaloosa, Alabama 35487

Roger L. Simpson
Department of Aerospace and Ocean Engineering, Virginia Tech, Blacksburg, Virginia 24061

Jonathan W. Newby
Department of Aerospace Engineering and Mechanics, The University of Alabama, Tuscaloosa, Alabama 35487

(Received 19 April 2005; accepted 20 December 2005; published online 21 February 2006)

A flow structure based triple-product correlation model developed by Nagano and Tagawa [J. Fluid Mech. **215**, 639 (1990)] has been expanded to three-dimensional turbulent flows. Three-dimensional turbulent boundary layer data obtained away from the vortex in a wing-body junction flow are analyzed to calculate the contributions from eight velocity octants to the stresses and higher-order products. The analysis showed that the sweep and ejection modes dominate the flow physics of some shear stresses and some triple products, while the interaction modes are negligible away from the wall. These experimental observations are used together with the extended Nagano-Tagawa mathematical model to obtain relations among the triple products in three-dimensional turbulent boundary layers that can simplify the turbulent diffusion modeling used in Reynolds-averaged Navier-Stokes equations. Results show that $\overline{\hat{u}^3}$, $\overline{\hat{u}^2\hat{v}}$, and $\overline{\hat{v}^3}$ triple product correlations can be modeled if an appropriate turbulence model is described for the $\overline{\hat{u}\hat{v}^2}$ triple product correlation, and that $\overline{\hat{u}^2\hat{w}}$ $\overline{\hat{v}^2\hat{w}}$ triple products correlations can be modeled if an appropriate turbulence model is described for the $\overline{\hat{u}\hat{v}\hat{w}}$ triple product correlation. © *2006 American Institute of Physics*. [DOI: 10.1063/1.2172650]

I. INTRODUCTION

The Reynolds-averaged Navier-Stokes equations require modeling of the turbulence diffusion and hence the triple products, among other terms. Many turbulence diffusion models used in computational fluid dynamics (CFD) codes, such as the models developed by Daly-Harlow,[1] Hanjalic-Launder,[2] Mellor-Herring,[3] and Lumley,[4] can be found in the literature. These turbulence diffusion models are the currently used models in turbulence closure as discussed by Launder and Sandham.[5] The models use the shear stresses, the gradient of the shear stresses, the turbulent kinetic energy dissipation rate, and the turbulent kinetic energy values to express the triple products. Experimental testing of these models, such as given by Schwarz and Bradshaw[6] for a three-dimensional turbulent boundary layer (3DTBL) and by Lemay *et al.*[7] in a manipulated 2DTBL, show that some of these models (Daly-Harlow and Mellor-Herring) are in good agreement only above $y^+=150$. These models require the turbulent-kinetic energy dissipation rate term as input, which results in large errors between the prediction and the data (Ölçmen and Simpson[8]). The turbulence diffusion term can be expressed as $[\mathrm{TD}_{ij}=-\partial(\overline{u_iu_ju_l})/\partial x_l]$, where "$u$" denotes the fluctuating velocity component, "x" denotes the coordinate axis, $i=1,2,3$ is the subscript denoting different coordinate axes, $l=1,2,3$ is the dummy subscript, and the overbar denotes Reynolds averaging. The tensor summation rule is required to use this equation.

The main motivation behind the current work was to gain more insights into the structure of the triple products and to obtain equations among the triple products that can simplify the turbulent diffusion modeling used in Reynolds-averaged Navier-Stokes equations. An analysis based on the work by Nagano and Tagawa[9,10] has been applied to data obtained at seven stations in a wing-body junction flow (Fig. 1) to investigate extending their analysis to three-dimensional (3D) flows.

In Sec. II, a brief description of the flow field is given. Mean velocity and normal stress profiles are presented. Contributions to the second- and third-order velocity products from a conditional averaging technique (octant analysis) using the signs of the velocity fluctuations as the discriminator are described next. Discussion on extending Nagano and Tagawa's model to three-dimensional boundary layers is given in Sec. III. Section IV describes the relations found between the triple products using the model together with the octant analysis results.

II. DESCRIPTION OF THE FLOW

The measurements used in this study were obtained in a wing/body junction flow in 1995 at Virginia Tech in the AOE Boundary Layer Wind Tunnel. The tunnel has an 8 m long test section with a 0.91 m wide by 0.25 m high rectangular cross section. The nominal free-stream air speed was 27.5 m/s and the free-stream turbulence intensity of the tun-

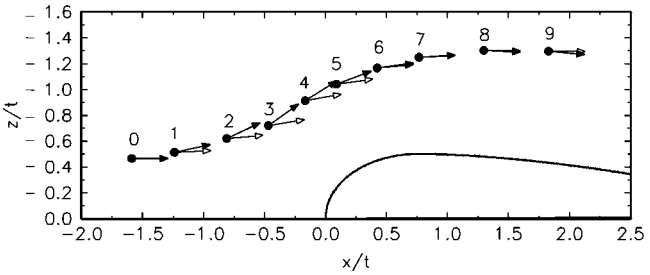

FIG. 1. Schematic figure of the wing-body junction. The dots show the measurement locations. Full arrows in wall-stress direction. Empty arrows in free-stream direction.

nel was less than 0.5%. The wing used was a 3:2 elliptical nose, NACA 0020 tailed wing profile with maximum thickness of 7.17 cm, a chord length of 30.5 cm, and a height of 23.2 cm (Fig. 1).

In a wing-body junction flow, the approach wall boundary layer separates from the wall and rolls toward the wing/wall junction to generate a vortical structure near the nose of the wing. This vortical structure wraps itself around the wing to generate a horseshoe vortex, which with the pressure gradient generated by the wing results in a highly three-dimensional flow field. Velocity measurements within the 3DTBLs developing on the floor of the tunnel were made using a three-simultaneous-component laser-Doppler velocimeter[11,12] that has a spherical measurement volume of 30 μm. In the study, six Reynolds stresses, ten triple products, and fifteen quadruple products were measured (Ölçmen and Simpson[11,12]) at seven stations, which were located outside the horseshoe vortex, and at each station data were obtained at 30 logarithmically spaced points by traversing the probe perpendicular to the wall. The approach boundary layer Reynolds number based on momentum thickness at 0.75 chord upstream of the wing was $\mathrm{Re}_\theta = 5940$. Table I gives the important characteristics of the flow field studied. Table II gives the uncertainties in the measured quantities.

The flow field around this particular wing is extremely well documented; detailed references for the flow data used in this study and data with different approach boundary layer Reynolds numbers are discussed in papers by Ölçmen and Simpson,[11–15] Simpson,[16,17] and references therein. All the Reynolds-averaged data used in this paper, including up to second-order products, the surface pressure measurements, and surface oil-flow visualizations, are presented by Ölçmen *et al.*[12,14] A brief description of the mean flow field and the Reynolds stress distribution is given here to aid in the discussion of the Nagano-Tagawa model.

In this paper, the data are used as represented in wall-stress coordinates where the x axis is along the wall-shear-stress direction on the tunnel wall pointing downstream and the y axis is perpendicular to the wall.

A. Mean flow field description

The U/u_τ profiles at all stations follow each other closely up to $y^+ = 9$ (Fig. 2). Above this height, station 1, 2, and 3 values closely follow each other up to $y^+ = 100$. These are the stations where three-dimensionality of the flow starts to develop. The U/u_τ profiles overlap each other with a semilogarithmic variation in the $y^+ = 30-150$ range, suggesting a similarity relation. At downstream stations, there is no similarity. Starting at station 4, the profiles become fuller and the semilogarithmic regions of the profiles shift to higher locations in the profiles.

Due to the definition of the wall-stress coordinates, the W/u_τ profiles are close to each other very near the wall with a magnitude of zero (Fig. 2). At the first three stations, W/u_τ monotonically increases from the wall to the layer edge since the flow in the entire layer turns in one direction. Between stations 3 and 4, the lateral pressure gradient in wall-stress coordinates changes sign. At station 4, the W/u_τ values are close to zero up to $y^+ = 40$. Above this y location, values monotonically increase. At stations further downstream, the effect of the sign change of the lateral pressure gradient is felt most near the wall. This results in negative W/u_τ values. The magnitude of the absolute maximum progressively increases downstream and the maximum points in the profiles shift upward in the layers. The Reynolds-averaged Navier-Stokes equations show that the mean flow is immediately affected by the mean pressure gradients. The pressure force is most effective on the near-wall flow where the momentum of the flow is lowest. The lateral pressure gradient in wall coordinates increases in magnitude proceeding downstream

TABLE I. Laser-Doppler velocimeter locations and flow parameters. Pressure coefficient gradients are calculated from the measured pressure distribution. U_e=Velocity magnitude at the layer edge. $\delta = y$ where $U/U_e = 0.995$=boundary layer thickness, $\delta_1 = \int_0^\infty (1 - U/U_e)dy$=streamwise displacement thickness, $\delta_2 = \int_0^\infty (1 - \sqrt{U^2 + W^2}/U_e)dy$=magnitude displacement thickness, $\delta_3 = \int_0^\infty (1 - U/U_e)U/U_e dy$=streamwise momentum thickness.

Stations	X (in)	Z (in)	U_{ref} (m/s)	U_e (m/s)	β_{FS} (deg)	β_w (deg)	u_τ (m/s)	v (m^2/s) x1E05	$\left(\frac{\partial C_p}{\partial x}\right)_{\mathrm{WC}}$ (1/m)	$\left(\frac{\partial C_p}{\partial z}\right)_{\mathrm{WC}}$ (1/m)	δ (mm)	δ_1 (mm)	δ_2 (mm)	δ_3 (mm)
1	−3.50	−1.45	27.5	24.9	−2.64	−11.5	0.864	1.65	0.9614	1.562	39.2	7.14	6.90	4.89
2	−2.29	−1.75	27.5	24.8	−4.81	−24.0	0.865	1.65	−0.75	2.898	40.2	9.14	7.54	6.30
3	−1.33	−2.04	27.5	25.3	−8.63	−33.7	0.957	1.65	−5.263	2.041	39.3	9.61	6.86	6.84
4	−0.47	−2.58	27.5	27.3	−9.45	−30.6	1.11	1.65	−6.264	−1.35	39	7.45	5.53	5.68
5	0.26	−2.94	27.5	29.5	−7.71	−19.7	1.15	1.67	−5.797	−3.036	39.6	5.95	5.37	4.66
6	1.19	−3.30	27.5	30.5	−5.09	−7.17	1.16	1.68	−3.999	−5.573	39.2	5.30	5.24	4.13
7	2.17	−3.53	27.5	31.0	−2.71	−3.50	1.20	1.68	0.58	−6.695	38.8	5.24	5.20	4.10

TABLE II. Uncertainties (±) in measured quantities with 20:1 odds.

U/u_τ	0.075	$\overline{u^2v}/(\overline{u^2})(\overline{v^2})^{1/2}$	0.020	$\overline{u^4}/(\overline{u^2})^2$	0.048
V/u_τ	0.026	$\overline{u^2w}/(\overline{u^2})(\overline{w^2})^{1/2}$	0.012	$\overline{u^3v}/(\overline{u^2})^{3/2}(\overline{v^2})^{1/2}$	0.139
W/u_τ	0.05	$\overline{v^2w}/(\overline{v^2})(\overline{w^2})^{1/2}$	0.011	$\overline{u^3w}/(\overline{u^2})^{3/2}(\overline{w^2})^{1/2}$	0.078
$\overline{u^2}/u_\tau^2$	0.08	$\overline{uv^2}/(\overline{u^2})^{1/2}(\overline{v^2})$	0.015	$\overline{u^2v^2}/(\overline{u^2})(\overline{v^2})$	0.039
$\overline{v^2}/u_\tau^2$	0.029	$\overline{uw^2}/(\overline{u^2})^{1/2}(\overline{w^2})$	0.009	$\overline{u^2vw}/(\overline{u^2})(\overline{v^2})^{1/2}(\overline{w^2})^{1/2}$	0.22
$\overline{w^2}/u_\tau^2$	0.037	$\overline{vw^2}/(\overline{v^2})^{1/2}(\overline{w^2})$	0.012	$\overline{u^2w^2}/(\overline{u^2})(\overline{w^2})$	0.034
$-\overline{uv}/(\overline{u^2v^2})^{1/2}$	0.023	$\overline{uvw}/(\overline{u^2})^{1/2}(\overline{v^2})^{1/2}(\overline{w^2})^{1/2}$	0.006	$\overline{uv^3}/(\overline{u^2})^{1/2}(\overline{v^2})^{3/2}$	0.073
$-\overline{uw}/(\overline{u^2w^2})^{1/2}$	0.021	$\overline{u^3}/(\overline{u^2})^{3/2}$	0.024	$\overline{uv^2w}/(\overline{u^2})^{1/2}(\overline{v^2})(\overline{w^2})^{1/2}$	0.023
$-\overline{vw}/(\overline{v^2w^2})^{1/2}$	0.018	$\overline{v^3}/(\overline{v^2})^{3/2}$	0.052	$\overline{uvw^2}/(\overline{u^2})^{1/2}(\overline{v^2})^{1/2}(\overline{w^2})$	0.023
		$\overline{w^3}/(\overline{w^2})^{3/2}$	0.022	$\overline{uw^3}/(\overline{u^2})^{1/2}(\overline{w^2})^{3/2}$	0.020
				$\overline{v^4}/(\overline{v^2})^2$	0.084
				$\overline{v^3w}/(\overline{v^2})^{3/2}(\overline{w^2})^{1/2}$	0.052
				$\overline{v^2w^2}/(\overline{v^2})(\overline{w^2})$	0.023
				$\overline{vw^3}/(\overline{v^2})^{1/2}(\overline{w^2})^{3/2}$	0.058
				$\overline{w^4}/(\overline{w^2})^2$	0.065

of station 4 up to station 7, and thus the effect of the pressure gradient is felt in a larger y range near the wall.

B. Normal stresses

The $\overline{u^2}/u_\tau^2$ normal stress profiles steeply increase from the wall to their peak at $y^+=15$ to 20 and then decrease up to $y^+=60$ to 450 at different stations (Fig. 3). The maximum in the profiles decreases up to station 4 due to adverse axial pressure gradient effects, and then increases back to station 1 values downstream due to the accelerating flow. However, above $y^+=100$, the values decrease monotonically downstream of station 1 up to station 7. The decrease at station 7 is approximately 60% of the station 1 value. This suggests that there are two zones in the flow where $\overline{u^2}$ is distinctly different: (1) below $y^+=100$, which is highly affected by the pressure gradients and wall proximity, and (2) above $y^+=100$, where the flow relaxes with more pronounced 3D effects.

Profiles of $\overline{v^2}/u_\tau^2$ monotonically increase to a maximum between $y^+=300$ and 400 and then decrease toward the freestream (Fig. 3). Downstream of station 1 up to station 5, the maximum value decreases. The station 6 maximum is higher than the maxima at stations 5 and 7.

The $\overline{w^2}/u_\tau^2$ profiles reach maxima at lower y^+ locations than the $\overline{v^2}/u_\tau^2$ stress profiles (Fig. 3). Values at station 2 and station 3 are higher with respect to station 1 values. Proceeding downstream up to station 7, the values decrease.

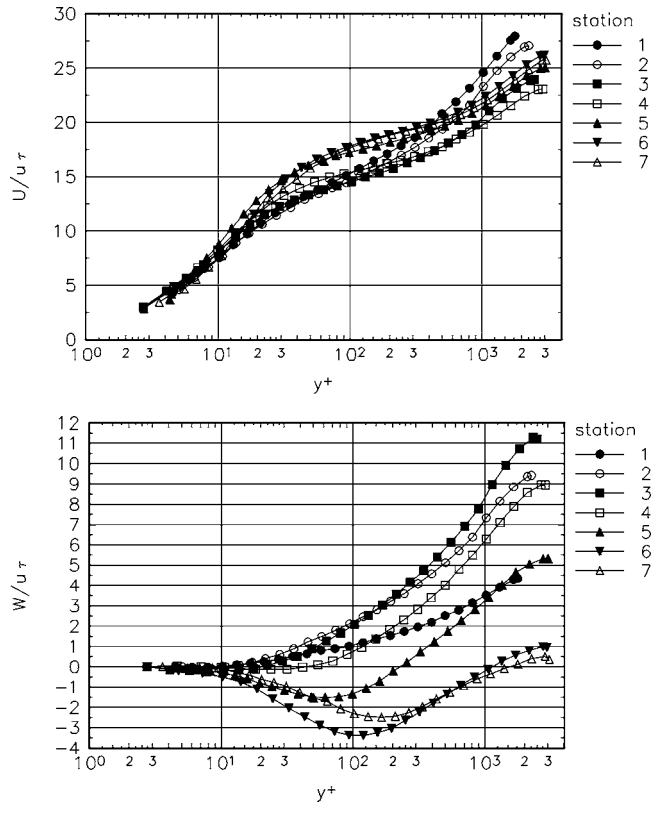

FIG. 2. U and W components of the velocity presented in wall-stress coordinates.

C. Second- and triple-order product correlations

1. Definitions of the octants

A conditional averaging technique was employed to calculate the Reynolds-averaged contributions from fluctuating velocity products to the overall Reynolds-averaged velocity product. Fluctuating velocity components with the specified combination of signs were used to calculate the contributions from each octant. The octants are defined using the signs of the fluctuating velocity components and are given in Table III. The octants resulting in positive $\overline{uv}$ value are named the interaction octants (octants 1, 3, 5, and 7), while the other octants are named the sweep-ejection octants.

2. Second- and triple-order product correlations

Second- and third-order products are discussed as nondimensionalized with the respective powers of the normal stresses. Figure 4 shows the nondimensional second-order product, the sum of the contributions from the interaction

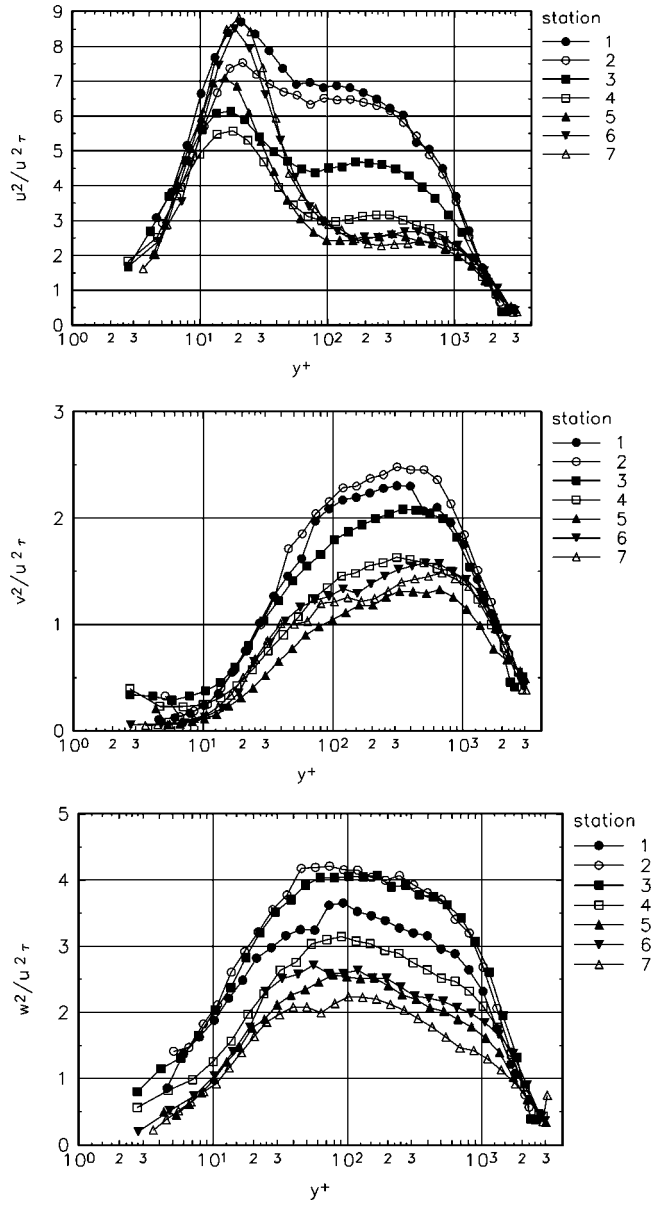

FIG. 3. The $\overline{u^2}/u_\tau^2$, $\overline{v^2}/u_\tau^2$, $\overline{w^2}/u_\tau^2$ normal stress component in wall-stress coordinates. The uncertainties are on the order of the symbol size.

TABLE III. Definition of the octants and the signs of the fluctuating velocity components in different octants.

Octant/Signs	u'	v'	w'
1 interaction	+	+	+
2 ejection	−	+	+
3 interaction	−	−	+
4 sweep	+	−	+
5 interaction	+	+	−
6 ejection	−	+	−
7 interaction	−	−	−
8 sweep	+	−	−

octants, and the sum of the contributions from the sweep-ejection octants obtained at station 5. Figure 5 shows similar plots for the triple product correlations. In this section, a qualitative comparison between the variations shown for station 5 and the other stations is given.

For the $\overline{uv}/(\overline{u^2v^2})^{1/2}$ second-order correlation, the sweep-ejection motion and the interaction motion contributions shown in Fig. 4 for station 5 represent the variations at every station. Although the contributions from the interaction motions are about 1/3 of the contributions from the sweep-ejection motion contributions, the contributions are not negligible.

At stations 1 through 3, the $\overline{uw}/(\overline{u^2w^2})^{1/2}$ correlation values become positive due to the fluctuating velocity field lagging behind the mean flow in readjusting its direction due to the lateral pressure gradients. While the mean flow monotonically turns in one direction, the fluctuating velocity field is less affected by the pressure gradients and persists in the free-stream direction resulting in +"w" fluctuations. In a similar fashion at stations 4 and downstream stations, the $\overline{uw}$ values become negative since the lateral pressure gradient sign change occurs between stations 3 and 4, and the near wall mean flow field starts turning toward the wall while the turbulence field persists in a direction closer to the free-stream flow direction. Above $y^+=100$, the $\overline{uw}$ values are positive (Fig. 4). The interaction motion contributions for this correlation become less in magnitude with values close to zero with increased three-dimensionality of the flow.

At every station, interaction motion contributions to the $\overline{vw}/(\overline{v^2w^2})^{1/2}$ correlation are effectively the same as presented for station 5 in Fig. 4, and are close to zero. Similar arguments made for the $\overline{uw}$ kinematic shear stress apply to the $\overline{vw}$ stress. The $\overline{vw}$ and the $\overline{uw}$ kinematic stresses are zero in 2DTBL. The lagging of the turbulence behind the mean flow results in positive values near the wall for stations 4 and downstream stations, while the values are less than zero throughout the layers for stations 1 through 3.

The $\overline{u^2v}/(\overline{u^2})(\overline{v^2})^{1/2}$ correlation peaks around $y^+=30$ (Fig. 5) and the peak value gradually increases proceeding from station 1 to 7, from about 0.075 to 0.25. The profile shape at every station stays effectively the same. Interaction octant contributions to the triple product value at different stations are effectively the same as shown for station 5 in Fig. 5.

$\overline{u^2w}/(\overline{u^2})(\overline{w^2})^{1/2}$ varies at every station similar to the variation of the quantity shown in Fig. 5 at station 5, except the changes observed below $y^+=30$. At stations 1 through 3, the negative peak value observed at $y^+=7$ at station 5 does not occur. Values stay positive and reduce monotonically toward the layer edge. At stations 4, 6, and 7, the negative peak values observed at $y^+=7$ are −0.02, −0.3, and −0.2. Near wall variation indicates that large "u" fluctuations occur together with intermittent large negative "w" fluctuations.

The $\overline{v^2w}/(\overline{v^2})(\overline{w^2})^{1/2}$ interaction octant contributions, as shown for station 5 in Fig. 5, are close to zero and similar variations are also observed at other stations. At stations 6 and 7 the triple product profiles show negative peaks at $y^+=15$, with values −0.15 and −0.2. However, the variations are similar to each other above $y^+=30$ at all stations.

Interaction octant contributions for the $\overline{uv^2}/(\overline{u^2})^{1/2}(\overline{v^2})$

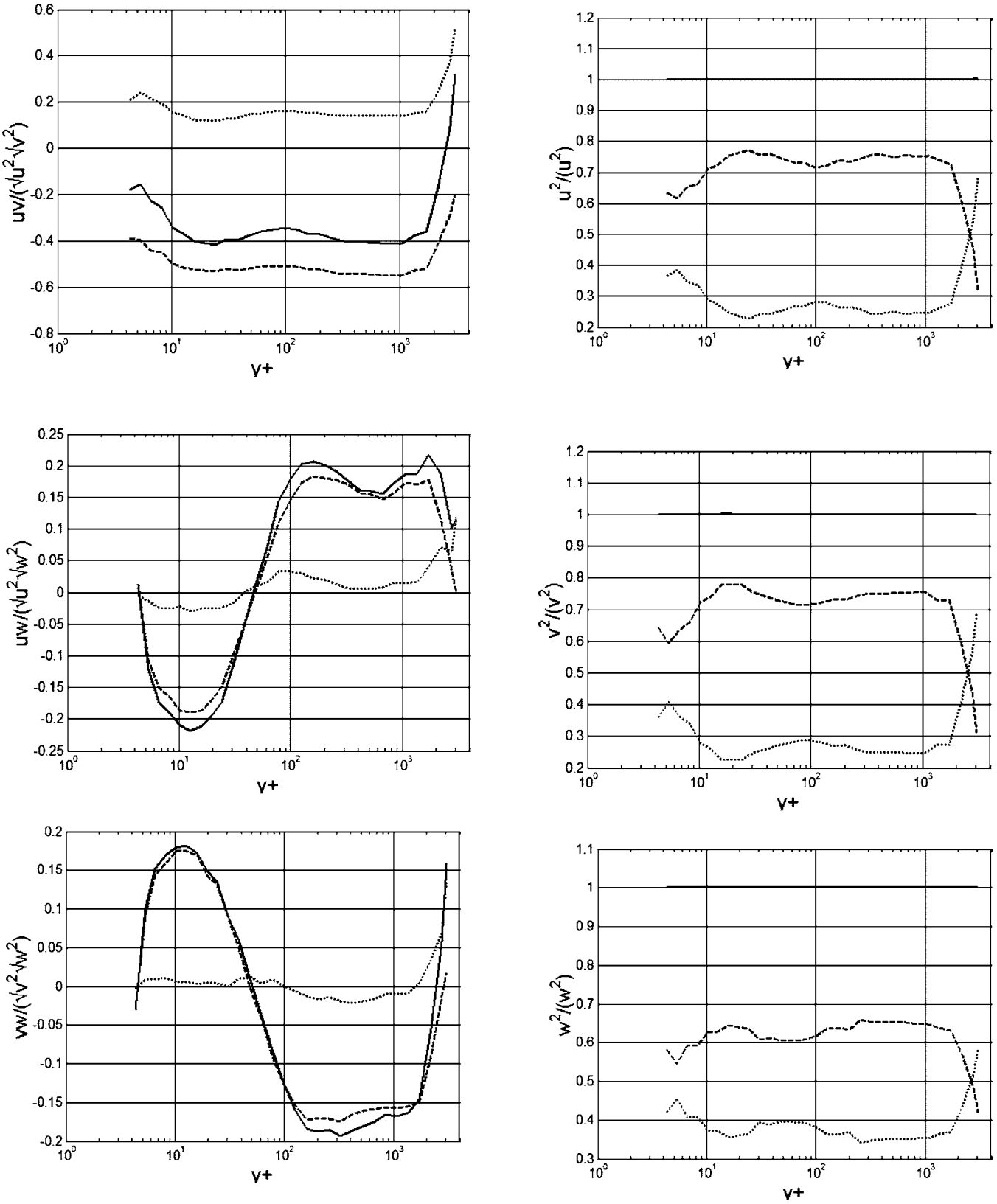

FIG. 4. Nondimensional second-order products and contributions from interaction and sweep/ejection octants for six second-order products presented for station 5. Solid line shows the nondimensional second-order product. Dashed line shows contributions from sweep/ejection octants modes. Dot-dash line shows contributions from interaction modes.

correlation are similar at every station with the values observed at station 5. At every station, the near wall peak observed at $y^+=8$ is between 0.3 and 0.4. However, the negative peak values are observed only at stations 5 and downstream stations. The negative peak values observed at $y^+=40$ are about −0.6 for station 6 and about −0.25 for station 7. Above $y^+=200$, the profiles vary in a similar fashion.

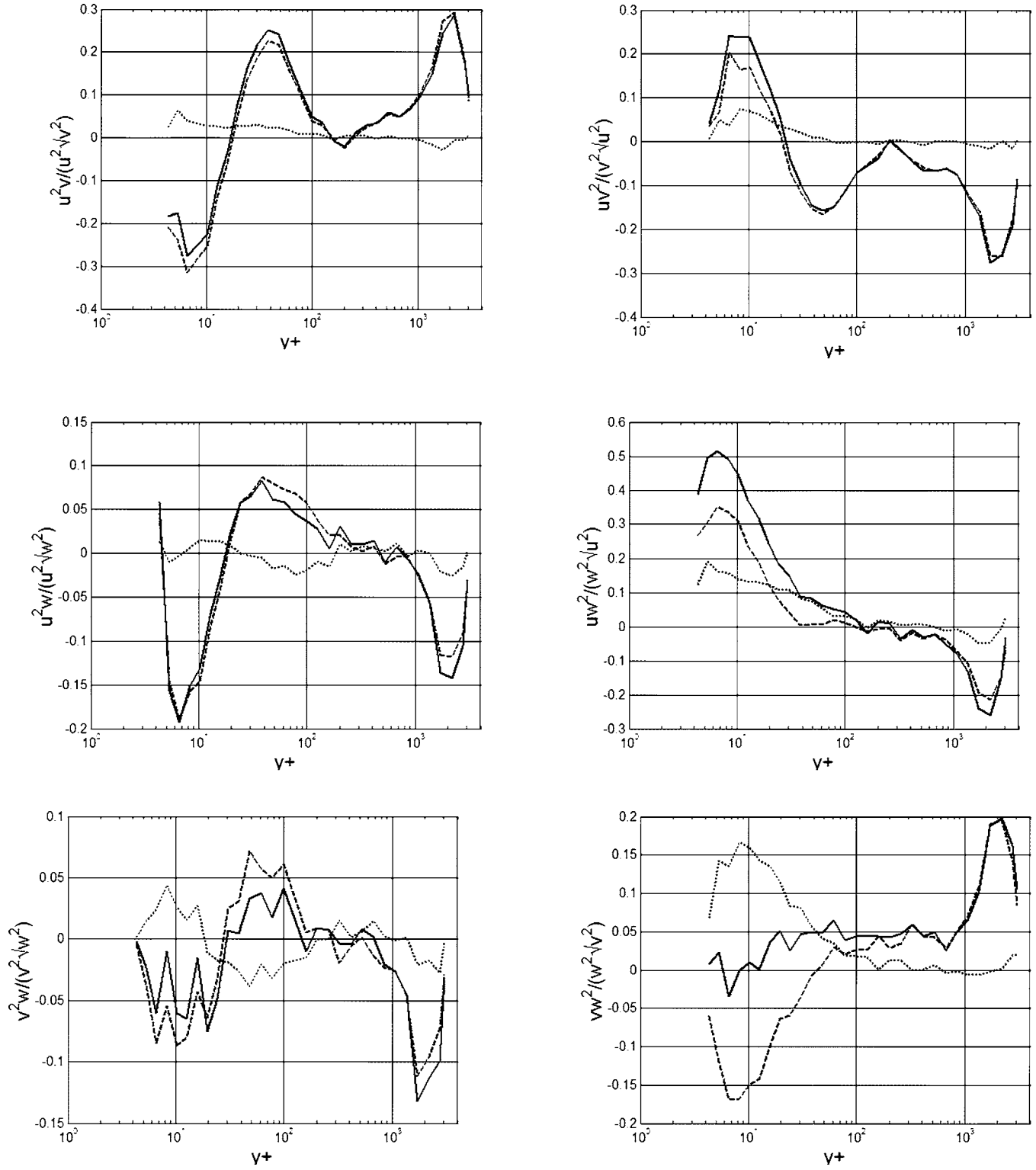

FIG. 5. Nondimensional triple products and contributions from interaction and sweep/ejection octants for ten triple products presented for station 5. Solid line shows the nondimensional triple product. Dashed line shows contributions from sweep/ejection octant modes. Dot-dash line shows contributions from interaction modes.

Interaction octant contributions for the $\overline{uw^2}/(\overline{u^2})^{1/2}(\overline{w^2})$ correlation are similar at every station to the values observed at station 5. Sweep-ejection contributions also show variations similar to the station 5 data with near wall values of about 0.25 at $y^+=7$ for all the stations except at station 5, where the value increases to 0.35, and at station 6, where it increases to 0.3.

Interaction octant contributions to the $\overline{vw^2}/(\overline{v^2})^{1/2}(\overline{w^2})$ correlation are close to zero above $y^+=100$ at all stations. The variations are qualitatively the same for all stations as

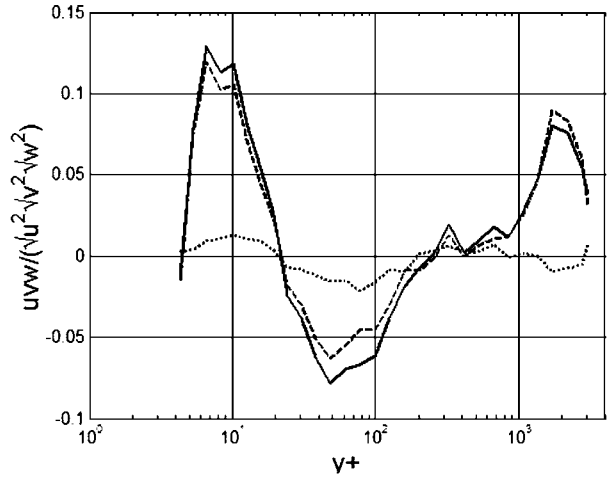

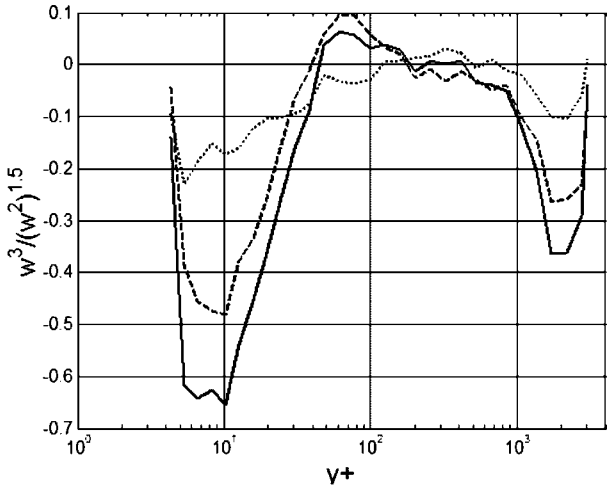

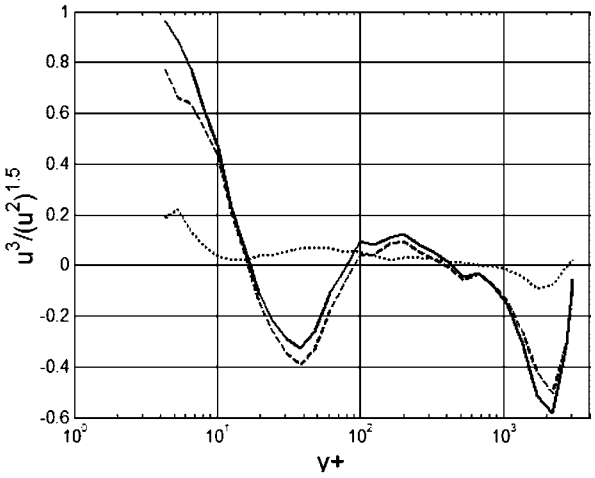

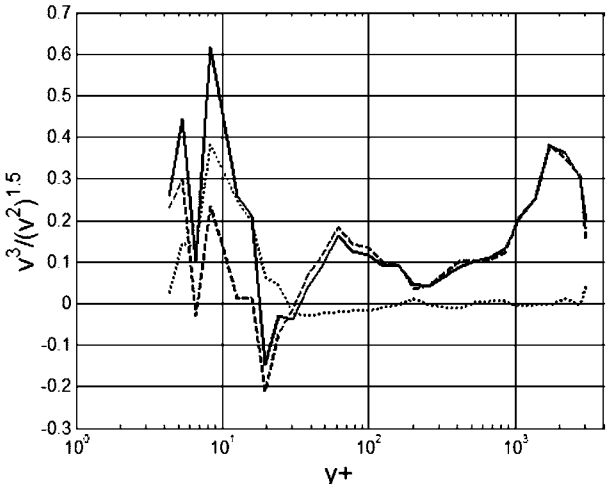

FIG. 5. (*Continued*).

observed at station 5. The contributions from the sweep-ejection octant contributions mirror each other with cumulative values close to but larger than zero at all stations. This motion indicates that "v" fluctuations occurring in the direction perpendicular to the floor occur both with ± "w" fluctuations without preference.

Interaction motion contribution shown for $\overline{uvw}/(\overline{u^2})^{1/2}(\overline{v^2})^{1/2}(\overline{w^2})^{1/2}$ in Fig. 5 also represents the variations at all the stations with values close to zero. The contributions from the sweep-ejection motions become significant for stations 3 and downstream stations. The positive peak around $y^+=10$ is about 0.15 at station 6 and is about 0.2 at

station 7. The negative peak observed at around $y^+=50$ develops proceeding downstream of station 3. The peak values are about −0.04 at station 4, about −0.08 at station 6, and about −0.04 at station 7. For stations 1 through 3, the near wall values are less than zero.

Interaction motion contributions to the $\overline{u^3}/(\overline{u^2})^{3/2}$ correlation are effectively the same at all stations. At stations downstream of station 4, while a peak positive value is observed below $y^+=10$, a negative peak starts forming and gradually the magnitude increases proceeding downstream. The peak values observed are about −0.05 at station 4 and about −0.3 at stations 5, 6, and 7. The negative peak formation affects the profiles in the $20<y^+<200$ range. Sweep-ejection motions are the dominant motions for this quantity.

For all the stations, sweep-ejection and the interaction motions contribute equally to the $\overline{v^3}/(\overline{v^2})^{3/2}$ correlation below $y^+=30$. Above $y^+=30$, the sweep-ejection motions are the dominant motions in the flow. The station 5 profile effectively represents the variations for all the other stations.

For the $\overline{w^3}/(\overline{w^2})^{3/2}$ correlation, the interaction and the sweep-ejection motion contributions are effectively the same throughout the layers at all stations. Except at stations 5, 6, and 7, the sweep-ejection contributions form a negative peak around $y^+=10$. The correlation values at $y^+=10$ is about −0.25 for station 4 and about −0.7 for stations 5, 6, and 7. While at stations 1 through 3 the correlation values gradually increase in the $y^+=10-500$ range, at the downstream stations the values reduce overall in the layers resulting in negative correlation values at station 7.

III. EXTENSION OF NAGANO-TAGAWA (REFS. 9 AND 10) MODEL FOR THREE-DIMENSIONAL FLOWS

As mentioned before, the main motivation behind the current work was to gain more insights into the structure of the triple products and to obtain equations among the triple products that can simplify the turbulent diffusion modeling used in Reynolds-averaged Navier-Stokes equations by extending the Nagano-Tagawa model to three-dimensional flows. The Nagano-Tagawa model is based on a non-Gaussian three-variable joint probability distribution expressed as an infinite series truncated at a chosen order. Using this probability distribution, Nagano and Tagawa first define equations for the individual quadrant contributions to each second- and third-order product in 2D flows as a linear function of various Reynolds-averaged second-, third-, and fourth-order products without using any experimental data in the derivation. Next, they obtain relations among the triple velocity correlations or among the velocity/temperature triple product correlations using the quadrant contribution equations and using experimental observations such as the sum of the interaction quadrant contributions to a triple product is zero. In this work, we first expand the Nagano-Tagawa model to three-dimensional flows and then use the model to express relations among the triple products in 3D flows based on experimental observations.

A. Extended model description

The statistical model developed by Nagano and Tagawa[9,10] for a 2DTBL with a passive scalar field describes a non-Gaussian three-dimensional joint probability density function using the velocity and temperature fluctuations. In the present work, we apply and extend their model to define a joint probability function (p.d.f.) using only the velocity field and use the p.d.f. to find relations between the triple velocity products using an octant analysis within a three-dimensional flow field.

The p.d.f. derived here is an algebraic equation for a three-dimensional joint probability density function as a function of the second-, third-, and fourth-order Reynolds-averaged velocity products, *without requiring prior knowledge of the experimental values* of the velocity products. Further use of the p.d.f., as described in the present section, gives algebraic equations for the fractional contributions from each of the eight octants to each of the second- and third-order velocity products. The octant contributions themselves are also expressed in terms of the second-, third-, and fourth-order velocity products without requiring the prior knowledge of the experimental values of the velocity products. These equations are later used together with experimental observations to define algebraic equations between the Reynolds-averaged triple products. For example, an experimental observation that can be made by studying the experimental data is that the sum of the interaction octant contributions for most of the triple-order products and the shear stresses are separately close to zero throughout the profiles at every station (Fig. 5).

B. Extended model derivation

The steps in the model development include (a) describing a characteristic function, which is the Fourier transform of the p.d.f that is being defined, (b) finding relations between the characteristic function and the fluctuating velocity products, (c) truncating the characteristic function such that the relations between the characteristic function and the velocity products include only up to fourth-order velocity products, and inverse Fourier transforming the characteristic function to obtain the p.d.f., and (d) expressing algebraic equations for the octant contributions for each of the second-order and the third-order products using the defined p.d.f.

The model uses the correlation coefficients rather than the actual value of the products. All of the velocity products were nondimensionalized with the respective powers of the normal stresses, $\overline{u^2}$, $\overline{v^2}$, $\overline{w^2}$ [e.g., $\overline{u^2v}$ was divided by $(\overline{u^2}\sqrt{\overline{v^2}})$, and is shown as $\overline{\hat{u}^2\hat{v}}=\overline{u^2v}/(\overline{u^2}\sqrt{\overline{v^2}})$]. Following their derivation and using the same notation, the extension of their model to three-dimensional flows can be described as follows:

(A) The Fourier transform of the joint p.d.f. $(P(\hat{u},\hat{v},\hat{w}))$ can be written as

$$\psi(\xi,\eta,\zeta)=\int_{-\infty}^{\infty}\int_{-\infty}^{\infty}\int_{-\infty}^{\infty}P(\hat{u},\hat{v},\hat{w}) \times\exp[i(\hat{u}\xi+\hat{v}\eta+\hat{w}\zeta)]d\hat{u}d\hat{v}d\hat{w}, \quad (1)$$

and one can obtain the three-dimensional joint p.d.f. by inverse transformation of the characteristic function, $\psi(\xi,\eta,\zeta)$, if a proper function is defined for the characteristic function. The function ψ was described by Nagano and Tagawa[9] in terms of the cumulant k_{pqr}, such that it would satisfy the following equation:

$$i^K k_{pqr}=\left.\frac{\partial^K \ln\psi(\xi,\eta,\zeta)}{\partial\xi^p\partial\eta^q\partial\zeta^r}\right|_{\xi=0,\eta=0,\zeta=0}, \quad (2)$$

where $K=p+q+r$, and ξ,η,ζ are the dummy variables. Integration of Eq. (2) led Nagano and Tagawa to the equation

$$\psi(\xi,\eta,\zeta)=\exp\left(\sum_{p,q,r=0}^{\infty}\frac{i^K}{p!q!r!}k_{pqr}\xi^p\eta^q\zeta^r\right). \quad (3)$$

Thus, this equation is the characteristic function $\psi(\xi,\eta,\zeta)$ chosen (Nagano and Tagawa[9]) to be used in Eq. (1).

(B) On the other hand, the Reynolds-averaged velocity corelations m_{pqr} can be expressed using the following relation:

$$m_{pqr}=\overline{\hat{u}^p\hat{v}^q\hat{w}^r}=\int_{-\infty}^{\infty}\int_{-\infty}^{\infty}\int_{-\infty}^{\infty}\hat{u}^p\hat{v}^q\hat{w}^r P(\hat{u},\hat{v},\hat{w})d\hat{u}d\hat{v}d\hat{w}. \quad (4)$$

The following equation holds between the function, ψ, given in Eq. (1) and the m_{pqr}, independent of Eqs. (2) and (3),

$$\left.\frac{\partial^K\psi(\xi,\eta,\zeta)}{\partial\xi^p\partial\eta^q\partial\zeta^r}\right|_{\xi=\eta=\zeta=0}=i^K m_{pqr}. \quad (5)$$

Integration of Eq. (5) leads to the function, ψ, expressed in terms of the m_{pqr}

$$\psi(\xi,\eta,\zeta)=\sum_{p,q,r=0}^{\infty}\frac{i^K}{p!q!r!}m_{pqr}\xi^p\eta^q\zeta^r. \quad (6)$$

Using the expressions for the ψ obtained in terms of m_{pqr} [Eq. (6)] and the k_{pqr} [Eq. (3)], one can calculate the following relations between m_{pqr} and k_{pqr} using up to fourth-order products. Although higher than fourth-order products could be used in the expressions, using terms including the fourth- and lower-order terms seems to be adequate in describing the probability density functions which are not Gaussian but those do not deviate largely from a Gaussian distribution (Nagano and Tagawa[9]). Therefore the $K=p+q+r\leqslant 4$ values are used here:

$$m_{001}=0;\quad m_{010}=0,\quad m_{100}=0;\quad m_{002}=1;\quad m_{020}=1;\quad m_{200}=1;\quad m_{000}=1,\quad k_{000}=0\quad \text{for}\quad K=0;$$

$$m_{\mathrm{pqr}}=k_{\mathrm{pqr}}\quad \text{for}\quad 1\leqslant K\leqslant 3;$$

$$k_{004}=-3+m_{004};\quad k_{013}=-3m_{011}+m_{013};$$

$$k_{022}=-1-2m_{011}^2+m_{022};\quad k_{031}=-3m_{011}+m_{031};\quad k_{040}=-3+m_{040};\quad k_{103}=-3m_{101}+m_{103};$$

$$k_{112}=-2m_{011}m_{101}-m_{110}+m_{112};\quad k_{121}=-m_{101}-2m_{011}m_{110}+m_{121};\quad k_{130}=-3m_{110}+m_{130};$$

$$k_{202}=-2m_{101}^2-m_{200}+m_{202};\quad k_{211}=-2m_{101}m_{110}-m_{011}m_{200}+m_{211};$$

$$k_{220}=-2m_{110}^2-m_{200}+m_{220};\quad k_{301}=-3m_{101}m_{200}+m_{301};\quad k_{310}=-3m_{110}m_{200}+m_{310};\quad k_{400}=-3+m_{400}.$$

(C) On the other hand, the ψ equation expressed in terms of k_{pqr} [Eq. (3)] can be further written as

$$\psi(\xi,\eta,\zeta)=\exp\left[-\frac{1}{2}(\xi^2+\eta^2+\zeta^2)\right]\sum_{p,q,r=0}^{\infty}C_{pqr}i^K\xi^p\eta^q\zeta^r. \quad (7)$$

This form of the ψ equation simplifies the inverse Fourier transform process required in calculation of the p.d.f. Taking the inverse Fourier transform of Eq. (7) results in the desired probability density function,

$$P(\hat{u},\hat{v},\hat{w})=\frac{1}{(2\pi)^3}\int_{-\infty}^{\infty}\int_{-\infty}^{\infty}\int_{-\infty}^{\infty}\psi(\xi,\eta,\zeta) \times\{\exp[-i(\hat{u}\xi+\hat{v}\eta+\hat{w}\zeta)]d\xi d\eta d\zeta\}$$
$$=\frac{1}{(2\pi)^{3/2}}\sum_{p,q,r=0}^{\infty}C_{pqr}H_p(\hat{u})H_q(\hat{v})H_r(\hat{w}) \times\left\{\exp\left[-\frac{1}{2}(\hat{u}^2+\hat{v}^2+\hat{w}^2)\right]\right\}, \quad (8)$$

where

$$H_k(\chi) = (-1)^k \exp\left(\frac{1}{2}\chi^2\right)\frac{d^k}{d\chi^k}\exp\left(-\frac{1}{2}\chi^2\right), \tag{9}$$

which is a one-dimensional Hermite polynomial.

Equations relating the k_{pqr} and C_{pqr} can be expressed using the ψ equation written in terms of k_{pqr} [Eq. (3)] and expanding it into series including the third-order terms in the expansion $\exp(x)=1+x+x^2/2!+x^3/3!$, and equating the terms from the ψ equation written in terms of C_{pqr} [Eq. (7)]. The C_{pqr} related to k_{pqr} can be expressed in terms of the m_{pqr}, which are the nondimensional Reynolds-averaged velocity products including the fourth-order terms. Again, following the reasoning by Nagano and Tagawa[9] the terms including the fourth-order terms have been retained here and higher-order terms have been neglected. The process results in the following relations:

$$C_{000}=1,\quad C_{001}=0,\quad C_{002}=0,\quad C_{003}=\tfrac{1}{6}\overline{\hat{w}^3},\quad C_{004}=\tfrac{1}{24}(\overline{\hat{w}^4}-3),$$

$$C_{010}=0,\quad C_{011}=\overline{\hat{v}\hat{w}},\quad C_{012}=\tfrac{1}{2}\overline{\hat{v}\hat{w}^2},\quad C_{013}=\tfrac{1}{6}(\overline{\hat{v}\hat{w}^3}-3\overline{\hat{v}\hat{w}}),\quad C_{020}=0,\quad C_{021}=\tfrac{1}{2}\overline{\hat{v}^2\hat{w}},\quad C_{022}=\tfrac{1}{4}(\overline{\hat{v}^2\hat{w}^2}-1),$$

$$C_{030}=\tfrac{1}{6}\overline{\hat{v}^3},\quad C_{031}=\tfrac{1}{6}(\overline{\hat{v}^3\hat{w}}-3\overline{\hat{v}\hat{w}}),\quad C_{040}=\tfrac{1}{24}(\overline{\hat{v}^4}-3),$$

$$C_{100}=0,\quad C_{101}=\overline{\hat{u}\hat{w}},\quad C_{102}=\tfrac{1}{2}\overline{\hat{u}\hat{w}^2},\quad C_{103}=\tfrac{1}{6}(\overline{\hat{u}\hat{w}^3}-3\overline{\hat{u}\hat{w}}),\quad C_{110}=\overline{\hat{u}\hat{v}},\quad C_{111}=\overline{\hat{u}\hat{v}\hat{w}},\quad C_{112}=\tfrac{1}{2}(\overline{\hat{u}\hat{v}\hat{w}^2}-\overline{\hat{u}\hat{v}}), \tag{10}$$

$$C_{120}=\tfrac{1}{2}\overline{\hat{u}\hat{v}^2},\quad C_{121}=\tfrac{1}{2}(\overline{\hat{u}\hat{v}^2\hat{w}}-\overline{\hat{u}\hat{w}}),\quad C_{130}=\tfrac{1}{6}(\overline{\hat{u}\hat{v}^3}-3\overline{\hat{u}\hat{v}}),\quad C_{200}=0,\quad C_{201}=\tfrac{1}{2}\overline{\hat{u}^2\hat{w}},\quad C_{202}=\tfrac{1}{4}(\overline{\hat{u}^2\hat{w}^2}-1),$$

$$C_{210}=\tfrac{1}{2}\overline{\hat{u}^2\hat{v}},\quad C_{211}=\tfrac{1}{2}(\overline{\hat{u}^2\hat{v}\hat{w}}-\overline{\hat{v}\hat{w}}),\quad C_{220}=\tfrac{1}{4}(\overline{\hat{u}^2\hat{v}^2}-1),\quad C_{300}=\tfrac{1}{6}(\overline{\hat{u}^3}),\quad C_{301}=\tfrac{1}{6}(\overline{\hat{u}^3\hat{w}}-3\overline{\hat{u}\hat{w}}),$$

$$C_{310}=\tfrac{1}{6}(\overline{\hat{u}^3\hat{v}}-3\overline{\hat{u}\hat{v}}),\quad C_{400}=\tfrac{1}{24}(\overline{\hat{u}^4}-3).$$

(D) Using the probability function given by Eq. (8), the fractional contributions from each octant to the $m_{pqr}=\overline{\hat{u}^p\hat{v}^q\hat{w}^r}$ can now be calculated using

$$(\overline{\hat{u}^l\hat{v}^m\hat{w}^n})_i=\sigma_{u,i}^l\sigma_{v,i}^m\sigma_{w,i}^n\left\{\int_0^\infty\left[\int_0^\infty\left(\int_0^\infty \hat{u}^l\hat{v}^m\hat{w}^n P(\sigma_{u,i}\hat{u}\sigma_{v,i}\hat{v}\sigma_{w,i}\hat{w})d\hat{w}d\hat{v}d\hat{u}\right)\right]\right\}, \tag{11}$$

where $\sigma_{u,i}=(1,-1,-1,1,1,-1,-1,1)$; $\sigma_{v,i}=(1,1,-1,-1,1,1,-1,-1)$; $\sigma_{w,i}=(1,1,1,1,-1,-1,-1,-1)$. Carrying out the integrals in Eq. (11) and retaining the terms including the fourth-order terms results in the following equation, which describes the fraction contributions to the $(\overline{\hat{u}^l\hat{v}^m\hat{w}^n})$ from separate octants:

$$(\overline{\hat{u}^l\hat{v}^m\hat{w}^n})_i=\frac{1}{(2\pi)^{3/2}}\sum_{p,q,r=0}^{K\leqslant 4}\sigma_{u,i}^{l+p}\sigma_{v,i}^{m+q}\sigma_{w,i}^{n+r}C_{pqr}B_{l,p}B_{m,q}B_{n,r}, \tag{12}$$

where

$$B_{j,k}=\int_0^\infty \chi^j H_k(\chi)\exp\left(-\frac{1}{2}\chi^2\right)d\chi. \tag{13}$$

The following terms were calculated using Eq. (13):

$$B_{0,0}=\sqrt{\frac{\pi}{2}},\quad B_{0,1}=1,\quad B_{0,2}=0,\quad B_{0,3}=-1,\quad B_{0,4}=0,\quad B_{1,0}=1,\quad B_{1,1}=\sqrt{\frac{\pi}{2}},\quad B_{1,2}=1,\quad B_{1,3}=0,\quad B_{1,4}=-1,$$

$$B_{2,0}=\sqrt{\frac{\pi}{2}},\quad B_{2,1}=2,\quad B_{2,2}=\sqrt{2\pi},\quad B_{2,3}=2,\quad B_{2,4}=0,\quad B_{3,0}=2,\quad B_{3,1}=3\sqrt{\frac{\pi}{2}}B_{3,2}=6,\quad B_{3,3}=6\sqrt{\frac{\pi}{2}},$$

$$B_{3,4}=6.$$

The derived equations differ from the equations given by Nagano and Tagawa since the integrations in Eq. (11) have different limits resulting in different constants for Eq. (12). Equation (12) as derived is coordinate-system-independent.

C. Extended model verification

The Nagano-Tagawa method, which was extended to three-dimensional flows, shows that the octant contributions to both the second- and third-order products are functions of the second-, third-, and fourth-order products in general. For example, the following two equations obtained using Eq. (12) show the contributions from octant-1 to the $(\overline{\hat{u}\hat{v}})$ second-order correlation and to the $(\overline{\hat{u}^2\hat{v}})$ triple-order correlation expressed using the Nagano-Tagawa analysis

$$(\overline{\hat{u}\hat{v}})_1 = \frac{1}{4\pi}\left[1 - \frac{\overline{\hat{v}\hat{w}^3}}{6} - \frac{\overline{\hat{v}^4}}{12} - \frac{\overline{\hat{u}\hat{w}^3}}{6} + \frac{\overline{\hat{u}\hat{v}^2\hat{w}}}{2} + \frac{\overline{\hat{u}^2\hat{v}^2}}{4} - \frac{\overline{\hat{u}^4}}{24} + \frac{\pi}{2}\overline{\hat{u}\hat{v}} + \frac{1}{\sqrt{2\pi}}\left\{-\frac{\overline{\hat{w}}^3}{3} + \overline{\hat{v}^2\hat{w}} + \pi\overline{\hat{u}\hat{v}\hat{w}} + \frac{\pi}{2}\overline{\hat{u}\hat{v}^2} + \overline{\hat{u}^2\hat{w}} + \frac{\pi}{2}\overline{\hat{u}^2\hat{v}}\right\}\right], \tag{14}$$

$$(\overline{\hat{u}^2\hat{v}})_1 = \frac{1}{4\pi}\left[\frac{\overline{\hat{w}^3}}{3} + \frac{\overline{\hat{v}^2\hat{w}}}{2} + 2\overline{\hat{u}\hat{v}\hat{w}} + \overline{\hat{u}\hat{v}^2} + \overline{\hat{u}^2\hat{w}} + \frac{\pi}{2}\overline{\hat{u}^2\hat{v}} + \frac{\overline{\hat{u}^3}}{3}\right] + \frac{1}{\sqrt{8\pi}}\left[\frac{5}{8} + \frac{\overline{\hat{v}\hat{w}}}{2} + \overline{\hat{u}\hat{v}} - \frac{\overline{\hat{v}\hat{w}^3}}{6} - \frac{\overline{\hat{v}^4}}{24} + \overline{\hat{u}^2\hat{v}\hat{w}} + \frac{\overline{\hat{u}^2\hat{v}^2}}{2} + \frac{\overline{\hat{u}^3\hat{v}}}{3}\right] + \frac{1}{(2\pi)^{3/2}}\left[\overline{\hat{u}\hat{w}} - \frac{\overline{\hat{u}\hat{w}^3}}{3} + \overline{\hat{u}\hat{v}^2\hat{w}} + \frac{\overline{\hat{u}^3\hat{w}}}{3}\right]. \tag{15}$$

The next step in extending Nagano and Tagawa's analysis is examination of the contributions from different octants to see if the derived equations represent the data. Figures 6 and 7 show the comparison between the model equations and the experimental data. The model values used in the plots were calculated by inputting the third- and fourth-order product correlation experimental data to the right-hand side of the equations, such as Eq. (14) or Eq. (15), and calculating the octant contributions as the left-hand side of the equations at every point in the profiles. Figure 6 shows a good agreement between the experimental and the modeled contributions to each of the second-order products and the eight octants for station five. Figure 7 also shows a good agreement between the model and the experimental data for each of the triple product correlations and the eight octants for station five. While only station five is shown, the other stations show good agreement with the model also.

IV. RESULTS AND DISCUSSION: STRUCTURAL MODELS FOR THIRD-ORDER PRODUCTS

The octant contribution equations expressed for the triple product correlation terms using the Nagano-Tagawa extended model were next used to express relations between the triple product correlations based on experimental observations. An experimental observation that can be made by studying the experimental data is that the sum of the interaction octant contributions for most of the triple-order products is separately close to zero throughout the profiles at every station (Fig. 5). In this study, a set of relations was obtained by summing the equations for the interaction octants of each of the triple product correlations separately and equating each sum to zero. Therefore, for each triple product correlation, the first, third, fifth, and seventh octant equations were added to each other and then equated to zero to obtain a relation. Ten such relations were obtained, one from each triple product correlation. Figure 5 also indicates the approximations made in writing such equations since the experimental data show that the interaction octant contributions are not exactly zero but close to it. Based on Fig. 5, it was also determined that for the $\overline{\hat{u}\hat{w}^2}$, $\overline{\hat{v}\hat{w}^2}$, and $\overline{\hat{w}^3}$, triple product correlation interaction octant contributions were not close to zero. Thus, it was observed that seven of those relations yielded good agreement with measured data. The seven relations were found from the equations for the triple product correlations, $\overline{\hat{u}^2\hat{v}}$, $\overline{\hat{u}^2\hat{w}}$, $\overline{\hat{u}^3}$, $\overline{\hat{u}\hat{v}^2}$, $\overline{\hat{u}\hat{v}\hat{w}}$, $\overline{\hat{v}^2\hat{w}}$, and $\overline{\hat{v}^3}$, and these relations are listed below in the order of the triple product correlation model equations used to obtain them:

$$\overline{\hat{u}\hat{v}^2} + \frac{\pi}{2}\overline{\hat{u}^2\hat{v}} + \frac{1}{3}\overline{\hat{u}^3} = 0, \tag{16}$$

$$\frac{\pi}{4}\overline{\hat{u}^2\hat{w}} + \overline{\hat{u}\hat{v}\hat{w}} = 0, \tag{17}$$

$$\overline{\hat{u}^2\hat{v}} - \frac{1}{9}\overline{\hat{v}^3} + \frac{\pi}{6}\overline{\hat{u}^3} = 0, \tag{18}$$

$$\overline{\hat{v}^3} + 3\overline{\hat{u}^2\hat{v}} + \frac{3\pi}{2}\overline{\hat{u}\hat{v}^2} = 0, \tag{19}$$

$$\overline{\hat{v}^2\hat{w}} + \overline{\hat{u}^2\hat{w}} + \pi\overline{\hat{u}\hat{v}\hat{w}} = 0, \tag{20}$$

$$\frac{\pi}{4}\overline{\hat{v}^2\hat{w}} + \overline{\hat{u}\hat{v}\hat{w}} = 0, \tag{21}$$

$$\pi\overline{\hat{v}^3} - \tfrac{2}{3}\overline{\hat{u}^3} + 6\overline{\hat{u}\hat{v}^2} = 0. \tag{22}$$

These seven equations, which contain seven triple product correlations, could not be solved to find relations among the correlations since the equations form a homogeneous set of equations without unique solutions. Additional relations were derived by using algebraic manipulations of the above relations to express each of the triple-product correlations as a function of only one other triple-product correlation, or to express each triple-product correlation as a function of other triple-product correlations. Such as, $\overline{\hat{u}^2\hat{v}} = -0.683\,\overline{\hat{u}^3}$ equation that can be obtained from Eqs. (16), (18), and (19), $-\frac{4}{3}\overline{\hat{v}^3} + \frac{\pi}{2}\overline{\hat{u}^3} - \frac{3}{2}\pi\overline{\hat{u}\hat{v}^2} = 0$ that can be obtained by eliminating the $\overline{\hat{u}^2\hat{v}}$ using Eqs. (18) and (19), and $\overline{\hat{u}^3} = -3\left(\overline{\hat{u}\hat{v}^2} + \frac{\pi}{2}\overline{\hat{u}^2\hat{v}}\right)$ that can be obtained from Eq. (16). Seventy-nine such equations were

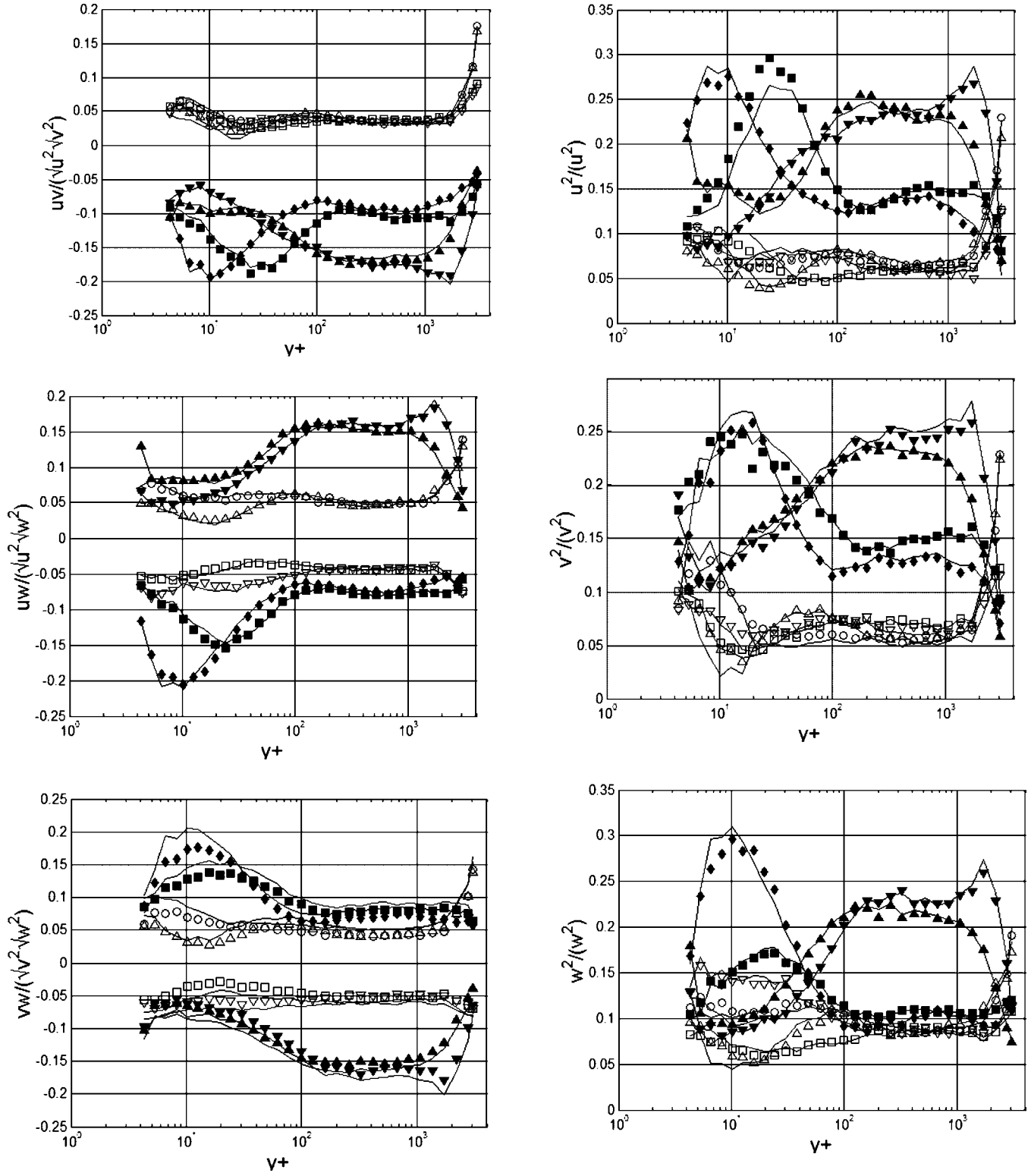

FIG. 6. Nondimensional second-order products, Nagano-Tagawa model predictions for each octant, contributions from each octant for six second-order products presented for station 5. Symbols show experimental data, octants 1 through 8, ○, ■, □, ▲, ▽, ▼, △, ♦. Solid lines following the symbols show octant contribution predictions using model.

expressed and tested against the data at seven stations. These equations were used to compute the model triple-product correlation values (the left-hand side of the equations) by inputting the required triple-product correlations from the experimental data to the right-hand side of the equations. Next the experimental value for the left-hand side term and the computed value were compared to each other.

To determine the model relations describing the data best, root-mean-square (rms) of the differences between the model predictions and the data was calculated for each rela-

tion using all the data of stations 1 through 7. The rms metric was next used to determine the relations best representing each of the seven triple-product-correlation data throughout the layers. Relations resulting in the least rms values were considered as the best relations. The best relations describing the variation of the triple product correlations for different y^+ ranges within the boundary layers were also determined from this analysis. The best working relations throughout the layers and at different regions within the layers are given in Table IV. Table V gives the normalized average rms value multiplied by 100 for the relations given in Table IV. The rms values calculated for each relation at each station were first normalized with the maximum value of the triple product at each station, next these seven rms values were aver-

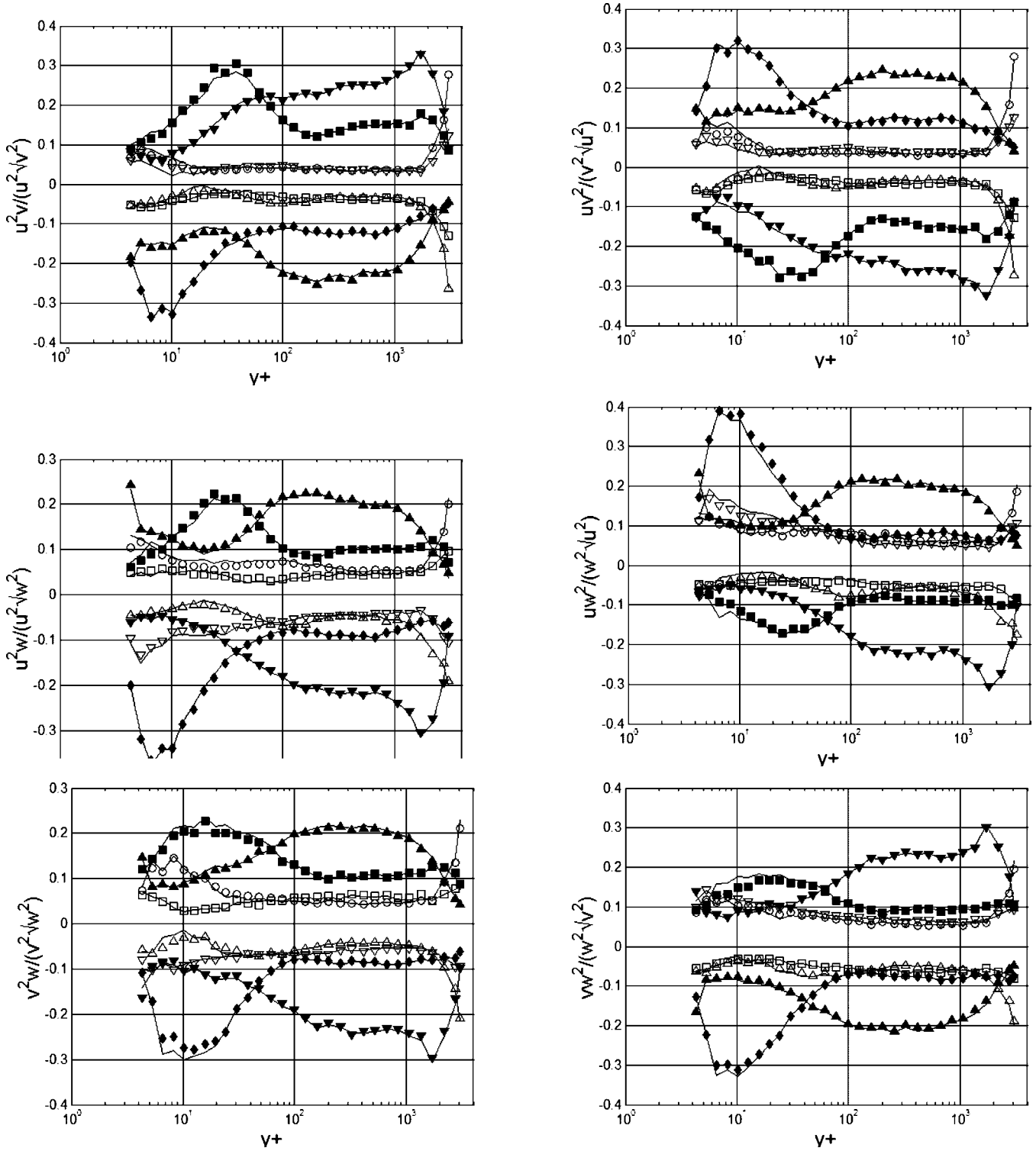

FIG. 7. Nondimensional triple products, Nagano-Tagawa model predictions for each octant, contributions from each octant for ten triple products presented for station 5. Symbols show experimental data, octants 1 through 8, ○, ■, □, ▲, ▽, ▼, △, ♦. Solid lines following the symbols show octant contribution predictions using model.

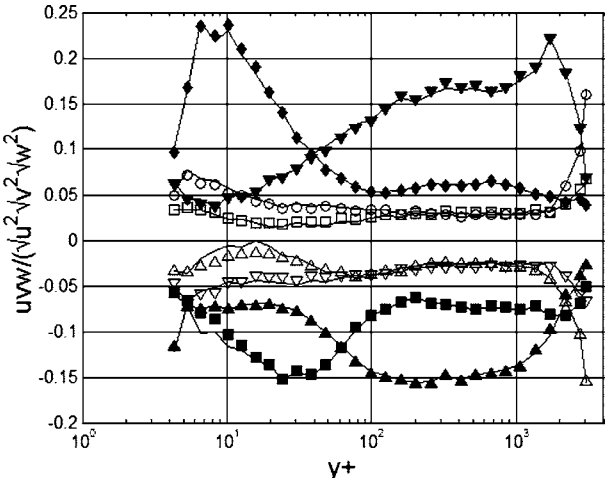

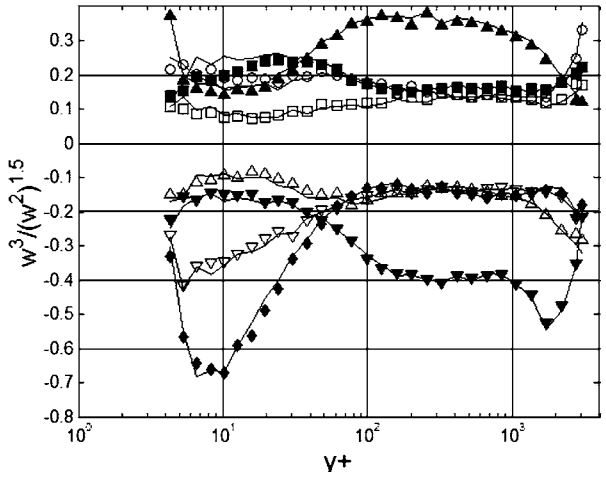

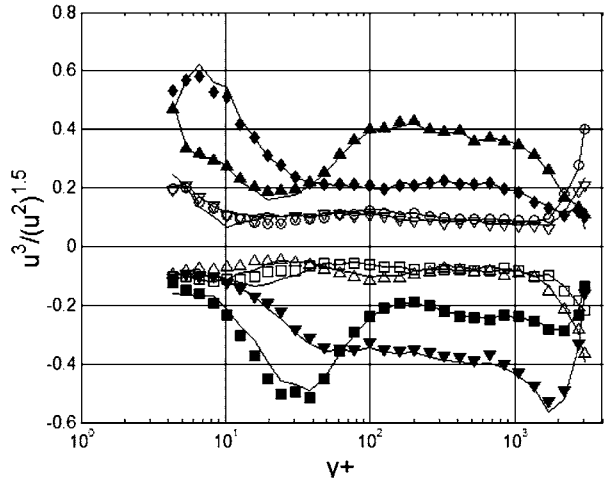

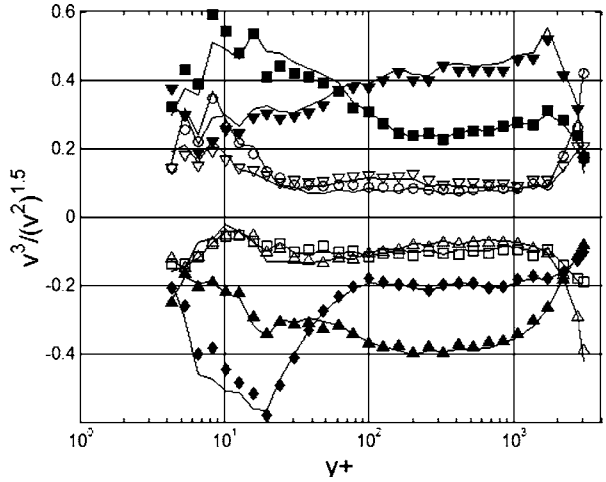

FIG. 7. (*Continued*).

aged to calculate the rms value reported for that relation. The values listed would serve the purpose of defining the percentage difference that might be expected in using the modeled equations.

Figure 8 shows the best working relations in different regions of the layers and the best working relation throughout the layer for each of the seven triple-product correlations for stations 2, 5, and 7 in comparison with the experimental data. The figure shows that both the relations that work best in different regions in the layers and the relations those work best on the average agree well with the data, with the specific region relation results being closer to the data. The plots also show that the model predictions and the data agree well throughout the layers for all the triple-product correlations

TABLE IV. Best working relations describing the variations of the triple product correlations. Average denotes the best working relation throughout the profiles at all stations. Best working relations in different regions of the layers are also shown in the table.

Triple-product correlation/ranges	Average	$y^+<30$	$30<y^+<300$	$y^+>300$
$\overline{\hat{u}^2\hat{v}}$	$\overline{\hat{u}^2\hat{v}}=-0.923^*\hat{u}\hat{v}^2$	$\overline{\hat{u}^2\hat{v}}=-0.923^*\hat{u}\hat{v}^2$	$\overline{\hat{u}^2\hat{v}}=-1.084^*\hat{u}\hat{v}^2$	$\overline{\hat{u}^2\hat{v}}=-0.5145^*\hat{u}^3$
$\overline{\hat{u}\hat{v}^2}$	$\overline{\hat{u}\hat{v}^2}=-\frac{2}{3\pi}(\overline{\hat{v}^3}+3\overline{\hat{u}^2\hat{v}})$	$\overline{\hat{u}\hat{v}^2}=-\frac{2}{3\pi}(\overline{\hat{v}^3}+3\overline{\hat{u}^2\hat{v}})$	$\overline{\hat{u}\hat{v}^2}=-\frac{2}{3\pi}(\overline{\hat{v}^3}+3\overline{\hat{u}^2\hat{v}})$	$\overline{\hat{u}\hat{v}^2}=-\frac{2}{3\pi}(\overline{\hat{v}^3}+3\overline{\hat{u}^2\hat{v}})$
$\overline{\hat{u}^3}$	$\overline{\hat{u}^3}=2.11^*\hat{u}\hat{v}^2$	$\overline{\hat{u}^3}=2.11^*\hat{u}\hat{v}^2$	$\overline{\hat{u}^3}=1.35^*\hat{u}\hat{v}^2$	$\overline{\hat{u}^3}=-1.945^*\overline{\hat{u}^2\hat{v}}$
$\overline{\hat{v}^3}$	$\overline{\hat{v}^3}=-1.463^*\overline{\hat{u}\hat{v}^2}$	$\overline{\hat{v}^3}=-1.463^*\overline{\hat{u}\hat{v}^2}$	$\overline{\hat{v}^3}=-1.463^*\overline{\hat{u}\hat{v}^2}$	$\overline{\hat{v}^3}=1.474^*\overline{\hat{u}^2\hat{v}}$
$\overline{\hat{u}^2\hat{w}}$	$\overline{\hat{u}^2\hat{w}}=-\frac{4}{\pi}(\overline{\hat{u}\hat{v}\hat{w}})$	$\overline{\hat{u}^2\hat{w}}=-1.869^*\overline{\hat{u}\hat{v}\hat{w}}$	$\overline{\hat{u}^2\hat{w}}=-\frac{4}{\pi}(\overline{\hat{u}\hat{v}\hat{w}})$	$\overline{\hat{u}^2\hat{w}}=-1.869^*\overline{\hat{u}\hat{v}\hat{w}}$
$\overline{\hat{v}^2\hat{w}}$	$\overline{\hat{v}^2\hat{w}}=0.6812^*\overline{\hat{u}^2\hat{w}}$	$\overline{\hat{v}^2\hat{w}}=-\frac{4}{\pi}(\overline{\hat{u}\hat{v}\hat{w}})$	$\overline{\hat{v}^2\hat{w}}=0.681^*\overline{\hat{u}^2\hat{w}}$	$\overline{\hat{v}^2\hat{w}}=0.681^*\overline{\hat{u}^2\hat{w}}$
$\overline{\hat{u}\hat{v}\hat{w}}$	$\overline{\hat{u}\hat{v}\hat{w}}=-\frac{1}{\pi}(\overline{\hat{v}^2\hat{w}}+\overline{\hat{u}^2\hat{w}})$	$\overline{\hat{u}\hat{v}\hat{w}}=-0.535^*\overline{\hat{v}^2\hat{w}}$	$\overline{\hat{u}\hat{v}\hat{w}}=-\frac{1}{\pi}(\overline{\hat{v}^2\hat{w}}+\overline{\hat{u}^2\hat{w}})$	$\overline{\hat{u}\hat{v}\hat{w}}=-\frac{1}{\pi}(\overline{\hat{v}^2\hat{w}}+\overline{\hat{u}^2\hat{w}})$

above y^+.20, except for the $\overline{\hat{v}^2\hat{w}}$ and the $\overline{\hat{u}\hat{v}\hat{w}}$ triple-product correlations for which the model predictions and the data agree better above y^+.100 and y^+.300, respectively. The percentage rms errors listed in Table V indicate that the models may result in large errors for all the triple products near the wall below y^+.30, at locations where the interaction octant contributions are not close to zero, and especially for the $\overline{\hat{v}^3}$, $\overline{\hat{u}^2\hat{w}}$, $\overline{\hat{v}^2\hat{w}}$ triple-product correlations. The rms errors decrease further away from the wall indicating the better agreement between the relations and the data.

The overall agreement between the relations and the data indicates that the relations expressed may be used to reduce the number of triple products in the modeling efforts of the turbulent diffusion. The relations given in Table IV may be used for this purpose. If a turbulence model equation for the $\overline{\hat{u}\hat{v}^2}$ term could be written, this could be used to model the $\overline{\hat{u}^3}$, $\overline{\hat{u}^2\hat{v}}$, and $\overline{\hat{v}^3}$ using the relations given in Table IV. Thus one turbulence model written for the $\overline{\hat{u}\hat{v}^2}$ could be used to model the additional three triple-product correlations. Additionally, if a turbulence model could be written for the $\overline{\hat{u}\hat{v}\hat{w}}$, this could be used to obtain a model for the $\overline{\hat{u}^2\hat{w}}$ and these equations together could be used to obtain a model for the $\overline{\hat{v}^2\hat{w}}$. Thus the diffusion modeling efforts for the triple products could be substantially reduced. Additionally the redundant equations for the $\overline{\hat{u}\hat{v}^2}$ and the $\overline{\hat{u}\hat{v}\hat{w}}$ in Table IV could be used as guiding equations to write the turbulence model equations for these correlations.

The relations obtained indicate that the triple-product terms, $\overline{u^2v}$, $\overline{uv^2}$, $\overline{v^3}$, which appear in the turbulence diffusion equations for the $\overline{u^2}$, $\overline{uv}$, and the $\overline{v^2}$ with the gradients normal to the wall are strongly related to each other even in this complex 3D flow. Another observation made from the relations is that one single relation was observed to hold for the $\overline{\hat{u}\hat{v}^2}$ at every region of the layers indicating a strong relation among the triple-product correlations. The equations involving $\overline{uw^2}$, $\overline{vw^2}$, and the $\overline{w^3}$ triple products are not presented here since the interaction octant contributions to these triple products were not close to zero especially in regions $y^+>150$.

The analysis discussed up to this point was also repeated in the local flow-angle coordinate system in which the x axis was aligned in the direction of the mean flow parallel to the wall at each point of the profiles, while the y axis was perpendicular to the tunnel wall. Therefore, a new coordinate system was defined at each point of the profiles. It was shown by Ha and Simpson[18] that in such a coordinate system the coherency of the axial velocity fluctuations is the highest, suggesting that coherent structures convected along the local flow-angle direction could result in interaction octant contributions closer to zero in the local flow-angle coordinates than in the wall-stress coordinates, especially near the wall. The results obtained in that coordinate system were observed to follow the results presented in wall-stress coordinates very closely without appreciable differences.

Although the relations developed here were tested in a single flow field, it is believed that the analysis would apply to any 3D boundary layer type flows. The flow field studied includes regions where the flow turns away in one direction to become a strongly skewed 3D flow and regions downstream where the flow turns in the opposite direction result-

TABLE V. Normalized root-mean-square errors multiplied by 100 calculated including all the seven stations for the equations given in Table IV in different regions of the layers. Average denotes the best working relation throughout the profiles at all stations.

Triple-product correlation/ranges	Average	$y^+<30$	$30<y^+<300$	$y^+>300$
$\overline{\hat{u}^2\hat{v}}$	14.4	23.4	11.6	7.78
$\overline{\hat{u}\hat{v}^2}$	14.2	27.2	8.0	9.6
$\overline{\hat{u}^3}$	13.7	20.7	10.9	5.56
$\overline{\hat{v}^3}$	22.5	40.7	16.1	9.4
$\overline{\hat{u}^2\hat{w}}$	33.8	56.8	25.8	19.1
$\overline{\hat{v}^2\hat{w}}$	59.2	89.6	47.4	33.6
$\overline{\hat{u}\hat{v}\hat{w}}$	16.6	25.7	15.6	10.4

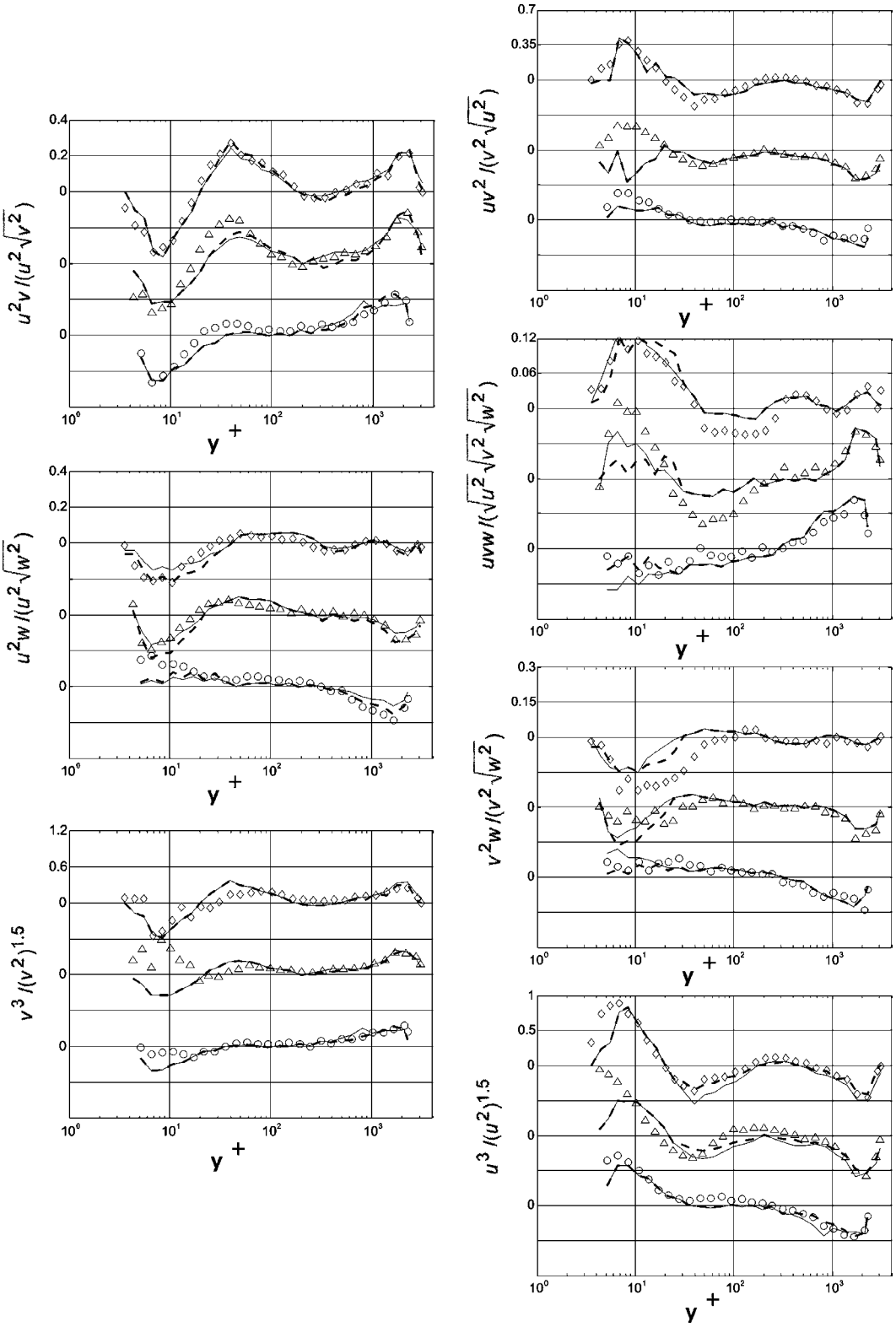

FIG. 8. Comparison between the predictions of models given in Table IV and the experimental data for stations 2, 5, and 7. Experimental data for stations 2, 5, and 7 are shown by ○, △, ◇ respectively. Thin lines show the model predictions for the best working relation on the average. Dashed lines show the relations working best in different regions of the layers.

ing in large lateral shear stresses and mean velocity gradients within the layers, encompassing phenomena that occur in most complex 3D flows.

A similar analysis made in the search of relations between the triple products using the octant contribution equations for the second-order products and using the assumptions that the sum of the interaction octant contributions is zero did not give any good relations that we could report,

although the experimental data show that the sum of the interaction octants for the $\overline{uv}$ and the $\overline{vw}$ stresses are nearly zero (Fig. 4).

V. CONCLUSIONS

The structural turbulence model for triple products developed by Nagano and Tagawa for two-dimensional flows is expanded to include three-dimensional flows. Algebraic model equations developed to express contributions from each of the octants to the triple products were first shown to successfully represent the octant contributions calculated using the experimental data. These model equations were further used together with experimental observations to express seven relations among the triple products. Experimental data analysis showed that for each of the seven triple products, the contributions from the interaction octants (octants, 1, 3, 5, 7) are much smaller in magnitude than the sweep/ejection octant contributions. The seven relations obtained by equating the sum of the model equations describing the contributions from the interaction octants to zero resulted in a homogeneous set of equations without unique solutions. Further equations were derived using these seven equations and a rigorous analysis was made to determine the best working relations that describe the triple products and thus relations among the triple products within different regions of layers as well as within the whole layers.

The analysis showed that a strong relation exists between the $\overline{\hat{u}\hat{v}^2}$, $\overline{\hat{v}^3}$, and $\overline{\hat{u}^2\hat{v}}$ triple-product correlations that hold in every region throughout the layers. Additional relations were expressed among the triple products that hold in different regions of the layers. These relations showed that the turbulent diffusion modeling can be substantially reduced by use of such relations expressed in Table IV. These relations show that $\overline{\hat{u}^3}$, $\overline{\hat{u}^2\hat{v}}$, and $\overline{\hat{v}^3}$ triple products can be modeled if an appropriate turbulence model is described for the $\overline{\hat{u}\hat{v}^2}$ triple product, and that $\overline{\hat{u}^2\hat{w}}$ $\overline{\hat{v}^2\hat{w}}$ triple products can be modeled if an appropriate turbulence model is described for the $\overline{\hat{u}\hat{v}\hat{w}}$ triple product. However, these relations were expressed using a single flow field generated by a wing-body junction, and further testing of these relations would allow further determination of the validity of these equations once additional three-dimensional flow data are available in the literature.

[1] B. J. Daly and F. H. Harlow, "Transport equations in turbulence," Phys. Fluids **13**, 2634 (1970).
[2] K. Hanjalic and B. E. Launder, "A Reynolds stress model of turbulence and its applications to asymmetric boundary layers," J. Fluid Mech. **52**, 609 (1972).
[3] G. L. Mellor and H. J. Herring, "A survey of mean turbulent field closure models," AIAA J. **11**, 590 (1973).
[4] J. L. Lumley, "Computation modelling of turbulent flows," Adv. Appl. Mech. **18**, 124 (1978).
[5] B. E. Launder and N. D. Sandham, *Closure Strategies for Turbulent and Transitional Flows* (Cambridge University Press, Cambridge, UK, 2002).
[6] W. R. Schwarz and P. Bradshaw, "Term-by-term tests of stress-transport turbulence models in a three-dimensional boundary layer," Phys. Fluids **6**, 986 (1994).
[7] J. Lemay, J. P. Bonnet, and J. Delville, "Experimental testing of diffusion models in a manipulated turbulent boundary layer," AIAA J. **33**, 1597 (1995).
[8] M. S. Ölçmen and R. L. Simpson, "Experimental evaluation of turbulent diffusion models in complex 3-D flow near a wing/body junction," AIAA Paper 97-0650 (1997).
[9] Y. Nagano and M. Tagawa, "Statistical characteristics of wall turbulence with a passive scalar," J. Fluid Mech. **196**, 157 (1988).
[10] Y. Nagano and M. Tagawa, "A structural turbulence model for triple products of velocity and scalar," J. Fluid Mech. **215**, 639 (1990).
[11] M. S. Ölçmen and R. L. Simpson, "A five-velocity-component laser-Doppler velocimeter for measurements of a three-dimensional turbulent boundary layer," Meas. Sci. Technol. **6**, 702 (1995).
[12] M. S. Ölçmen, R. L. Simpson, and J. George, "Some Reynolds number effects on two- and three-dimensional turbulent boundary layers," Exp. Fluids **31**, 219 (2001).
[13] M. S. Ölçmen and R. L. Simpson, "Perspective: On the near wall similarity of three-dimensional turbulent boundary layers," J. Fluids Eng. **114**, 487 (1992).
[14] M. S. Ölçmen and R. L. Simpson, "An experimental study of a three-dimensional pressure-driven turbulent boundary layer," J. Fluid Mech. **290**, 225 (1995).
[15] M. S. Ölçmen and R. L. Simpson, "Some features of a turbulent wing-body junction vortical flow," AIAA Paper 97–0651, presented at the 35th Aerospace Sciences Meeting and Exhibit, Reno, NV, 6–10 January 1997.
[16] R. L. Simpson, "Aspects of turbulent boundary layer separation," Prog. Aerosp. Sci. **32**, 457 (1996).
[17] R. L. Simpson, "Junction flows," Annu. Rev. Fluid Mech. **33**, 415 (2001).
[18] S. Ha and R. L. Simpson, "An experimental investigation of a three-dimensional turbulent boundary layer using multiple-sensor probes," Ninth Symposium on Turbulent Shear Flows, Kyoto, Japan, 16–18 August 1993, p. 2-1-(1–6); VPI-AOE-205, DTIC.